Microchimica Acta (2018) 185: 43
https://doi.org/10.1007/s00604-017-2596-2

ORIGINAL PAPER

Immobilization of zirconium-glycerolate nanowires on magnetic nanoparticles for extraction of urinary ribonucleosides

Jing Xu[1] · Zheng Zhang[1,2] · Xiao-Mei He[1] · Ren-Qi Wang[1,3] · Dilshad Hussain[1,4] · Yu-Qi Feng[1]

Received: 16 August 2017 / Accepted: 29 November 2017 / Published online: 8 December 2017

Abstract

The authors have immobilized nanowires made from zirconium glycerolate (ZrGly) on magnetite (Fe_3O_4) nanoparticles by applying a solvothermal growth process using metal-glycerolate as a precursor. The structure and the dissolution-recrystallization mechanism of the resulting Fe_3O_4@ZrGly composite were investigated by attenuated total reflection-FTIR, energy-dispersive X-ray analysis, thermogravimetric analysis and solid-state cross polarization/magic angle spinning ^{13}C NMR spectroscopy. The interaction between the zirconium glycerolate in Fe_3O_4@ZrGly and *cis*-diols leads to efficient adsorption of ribonucleosides which then can be quantified by HPLC with UV detection. The sorbent was successfully applied to the selective enrichment of adenosine, cytidine, uridine and guanosine from spiked human urine samples. The detection limit of the method is in the range from 1.7 to 19 ng·mL^{-1} of nucleosides in spiked human urine, with relative standard deviations of lower than 12.4% and recoveries ranging from 90.6 to 113%.

Keywords Organic-metal nanowire · Immobilized metal ion affinity chromatography · *Cis*-diols · Matrix interference · One-pot solvothermal synthesis · Dissolution-recrystallization formation mechanism · Langmuir adsorption mechanism · Coordination interaction · ZrO_2 · CeO_2

Introduction

Ribonucleosides in urines have been considered as potential biomarkers for early cancer diagnostics [1]. However, these *cis*-diol biomolecules are normally present in complex matrix with sub-stoichiometric amounts, and thus proper enrichment is indispensable before detection. So far, lectin affinity chromatography [2], hydrazide chemistry [3], hydrophilic interaction chromatography [4], boronate affinity chromatography [5–8] have been developed for such a purpose. However, the complicating operation of lectin affinity chromatography and hydrazide chemistry is time-consuming. Meanwhile, boronate affinity materials often require multiple synthesis steps, which complicates their applications [9–11]. Metal oxide affinity chromatography has also been successfully employed for the separation of *cis*-diol biomolecules due to their unique amphoteric properties, good mechanical strength and chemical stability. Specifically, ZrO_2 has been successfully used for the enrichment of *cis*-diol biomolecules, due to the high affinity and excellent specificity [12]. Nonetheless, the time costing centrifuge process and nonspecific adsorptions are still flaws when it is used in the analysis of biological samples.

The appearance of magnetic solid phase extraction technology (MSPE) takes place of the nagging centrifuge process. Thus, magnetic nanomaterials have attracted intense research interests in sample preparation [13]. However, low mass transfer efficiency, poor biocompatibility and

Presented at the 30th annual academic meeting of China Chemical Society, Dalian, China, 1–4 July 2016.

Electronic supplementary material The online version of this article (https://doi.org/10.1007/s00604-017-2596-2) contains supplementary material, which is available to authorized users.

✉ Yu-Qi Feng
yqfeng@whu.edu.cn

[1] Key Laboratory of Analytical Chemistry for Biology and Medicine (Ministry of Education), Department of Chemistry, Wuhan University, Wuhan 430072, China

[2] State Key Laboratory of Proteomics, Beijing Proteome Research Center, Beijing Institute of Radiation Medicine, Beijing 102206, China

[3] College of Chemistry and Chemical Engineering, Lanzhou University, Lanzhou 730000, China

[4] Division of Analytical Chemistry, Institute of Chemical Sciences, Bahauddin Zakariya University, Multan (60800), Pakistan

serious interference of nonspecific adsorption on magnetic nanomaterials limit their applications under physiological conditions [14]. To circumvent these obstacles, Fe_3O_4 with 1D porous nanostructure was fabricated, providing short transport path and efficient mass transfer along the confined radial dimension [15]. Unfortunately, immobilizing *c*is-diol functional materials on the surface of Fe_3O_4 is still a challenge considering their low chemically activity. Multistep methods have been developed for functionalizing 1D nanostructures such as electrochemical deposition [16], homogeneous precipitation [17] and inorganic or polymer template directed synthesis [18]. Nevertheless, the processes of such methods involve relatively tedious synthetic procedures and rigorous experimental conditions. Thus, it is highly desirable to immobilize high-quality 1D nanostructures with good selectivity and magnetic property simultaneously in more convenient manner.

This work describes a strategy based on a precursor-induced solvothermal growth process, for the synthesis of Fe_3O_4-zirconium-glycerolate (Fe_3O_4@ZrGly). The dissolution-recrystallization formation mechanism of Fe_3O_4@ZrGly was investigated. Furthermore, the Langmuir adsorption model verified a monolayer adsorption mechanism between Fe_3O_4@ZrGly and adenosine through coordinative interactions. In addition, the prepared material showed higher selectivity towards ribonucleotides in the presences of *cis*-diol analogue glucose or horseradish peroxidase (HRP). Finally, it was successfully applied on the selective extraction of ribonucleotides from human urine.

Experimental

Materials and chemicals

Zirconium acetylacetone ($C_{20}H_{28}O_8Zr$), ZrO_2 (Z104401–100 g), CeO_2 (C03980–25 g) were purchased from Aladdin Chemical Co. Ltd. (Shanghai, China, http://www.aladdin-e.com). Glycerol, ethanol, ammonium formate ($HCOONH_4$), aqueous ammonia solution ($NH_3{\cdot}H_2O$, 25 wt%) were supplied by Shanghai General Chemical Reagent Factory (Shanghai, China, http://www.sinoreagent.com). Trifluoroacetic acid (TFA) and d_6-dimethyl sulfoxide (d_6-DMSO) were purchased from Sigma-Aldrich (St. Louis, USA, http://www.sigmaaldrich.com). 2′-deoxyadenosine (dA), 2′- deoxycytidine (dC), cytidine (C), guanosine (G), adenosine (A) and uridine (U) were purchased from Sigma-Aldrich (Beijing, China, http://www.sigmaaldrich.com). HPLC grade methanol (CH_3OH) was obtained from Fisher Scientific (Pittsburgh, USA). Purified water was obtained on a Milli-Q apparatus (Millipore, Bedford, MA, USA, http://www.millipore.bioon.com.cn).

Preparation of zirconium-glycerolate modified Fe_3O_4 nanoparticles (Fe_3O_4@ZrGly) and zirconium-glycerolate nanowire (ZrGly)

Fe_3O_4 particles were prepared according to reference [19]. For the preparation of Fe_3O_4@ZrGly, 200 mg of $C_{20}H_{28}O_8Zr$ (0.4 mmol) and 4 g of glycerol (44 mmol) were mixed in a 40 mL polytetrafluoroethylene autoclave to form a milky solution. Thereafter, 200 mg Fe_3O_4 particles were suspended in 20 g C_2H_5OH (434 mmol) by ultrasonication for 5 min. Subsequently, Fe_3O_4 suspension was mixed with the milky solution and subjected to a solvothermal process at 200 °C for 15 h. The product Fe_3O_4@ZrGly was washed with ethanol and dried at 80 °C for 4 h. Pure ZrGly was also prepared under the same conditions without the addition of Fe_3O_4 for the comparison.

Acid dissolution test for ZrGly

An acid dissolution test was carried out by dispersing 50 mg ZrGly powder samples in TFA aqueous solution (10 vt%, 4 mL). After shaking for 30 min, the supernatant was collected and evaporated to dryness under a mild nitrogen stream at 40 °C. Finally, the residue was re-dissolved in 600 μL d_6-DMSO for ^{13}C–NMR analysis.

Adsorption capacity evaluation

Taking the coordination interaction between zirconium and *cis*-diol groups into account, adenosine was chosen as a probe to investigate the adsorption mechanism. 5 mg of Fe_3O_4@ZrGly, ZrO_2 or CeO_2 was incubated with a series of $NH_3{\cdot}H_2O$ solutions (0.5 vt %, 4 mL) of adenosine for 4 h. The concentrations of adenosine ranged from 0 to 500 $\mu g{\cdot}mL^{-1}$. Supernatants were injected for HPLC analysis. The equilibrium adsorption amount (q_e, $mg{\cdot}g^{-1}$) was calculated according to the following formula:

$$q_e = \frac{(C_0 - C_e) * V}{m} \quad (1)$$

where c_0 and c_e ($mg{\cdot}mL^{-1}$) are the concentration of adenosine solution before and after adsorption; V (mL) is the volume of the adenosine solution; m (g) is the mass of the adsorbents.

Dispersive solid-phase extraction procedure

For each extraction, 5 mg of Fe_3O_4@ZrGly was added to 100 μL of ribonucleosides mixture (2 $\mu g{\cdot}mL^{-1}$ for each nucleoside, dissolved in 0.5 vt % $NH_3{\cdot}H_2O$ solutions), and the mixture was vortexed at room temperature for 5 min. The material with captured ribonucleosides was separated from

the mixed solutions via an external magnet. After washing twice with 1 mL of water, the trapped ribonucleosides were eluted with 1 mL of 0.1 vt % FA in water. The eluent was collected and lyophilized to dryness with a centrifugal vacuum concentrators (Labconco, Kansas City, MO, USA). The residue was dissolved in water (100 μL) for chromatographic analysis. For comparison, Fe_3O_4 was also used for the extraction of ribonucleosides according to the same procedure.

Selectivity evaluation

Loading solutions containing adenosine (*cis*-diol, 2 μg·mL^{-1}) and deoxyadenosine (non-*cis*-diol, μg·mL^{-1}), adenosine (*cis*-diol, 2 μg·mL^{-1}) and glucose (*cis*-diol, μg·mL^{-1}), adenosine (*cis*-diol, 2 μg·mL^{-1}) and HRP(*cis*-diol, μg·mL^{-1}) were used to investigate the selectivity of Fe_3O_4@ZrGly, respectively. 0.1 mL these solutions was incubated with Fe_3O_4@ZrGly (5 mg) for 5 min. The initial solution before and after extraction were injected into the chromatographic system. The process was repetitively conducted with 1-fold, 5-fold, 50-fold and 500-fold (1-fold, 10-fold and 100-fold in the case of glucose and HRP) excesses of the interfering analog to determine the ability of Fe_3O_4@ZrGly to capture ribonucleosides from complex samples.

Urine samples preparation

Human urine samples were collected from 2 healthy female volunteers with 25 years old and stored at −20 °C until use. After centrifugation, urine sample was diluted with 0.5 vt% $NH_3{\cdot}H_2O$ solution at a ratio of 1:9 (*v*/v), and then mixed with a vortex mixer. The obtained mixture was centrifuged for 10 min at 14000 g, and the supernatant was used for the extraction procedure. Spiked sample was prepared by addition of nucleoside standards in urine.

Results and discussion

Choice of materials

The Fe_3O_4@ZrGly nanoparticles were designed to cope with the following state-of-art technique limits. Firstly, the phenyl group of boronate affinity adsorbents can introduce serious secondary interactions (hydrophobic interaction) which may result in the adsorption of hydrophobic interferent and largely decrease its selectivity to ribonucleosides [20]. As for commercial metal oxide adsorbents (like ZrO_2 and CeO_2), heterogeneous adsorption sites also lead to nonspecific adsorption, which often cause serious matrix interference in analysis of practical samples. On the contrary, glycerol acted as a linear template and stabilizer for zirconium acetylacetone. It occupied the adsorption sites of zirconium ions and homogenized the surface of Fe_3O_4@ZrGly. Figure S4 proved that the coordination only exists between Fe_3O_4@ZrGly and ribonucleosides. Although the recoveries of ribonucleosides reduce in this way, it endows the material with higher selectivity simultaneously. Secondly, the introduction of 1D organic metal nanowires prominently enlarges the surface area of Fe_3O_4 (from 14 to 142 $m^2{\cdot}g^{-1}$). The adsorption capacity is equal to that of commercial ZrO_2, while better than commercial CeO_2. Thirdly, the one pot strategy of immobilization is inexpensive than the synthesis of mostly boronate affinity adsorbents, which are time-consuming and costly to prepare because of the requirements of multiple reactions. It's also more convenient than traditional method like sol-gel, which need strict experiment condition and abundant experience. Magnetic hierarchical architectures containing organic metal nanowires can form by the one-pot solvothermal reaction. Fourthly, the magnetism of Fe_3O_4@ZrGly improves the efficiency. A typical extraction procedure can be finished within 10 min.

Characterizations

The morphologies of the Fe_3O_4, ZrGly and Fe_3O_4@ZrGly were examined by TEM and SEM. Fe_3O_4 nanospheres presented a spherical morphology with average diameter of 211 ± 22 nm (n = 80, Fig. S1a, d). The bare ZrGly nanowires are 5–15 nm in diameter and at least 30 nm in length (Fig. S1b, e). After immobilizing ZrGly nanowires onto Fe_3O_4 nanospheres, the morphology of Fe_3O_4 remain their original shape, but the size increase to 218 ± 19 nm (n = 73, Fig. S1c, f) causing by the introduction of ZrGly. The streaky layer distributes around the Fe_3O_4 core indicated the synthesis strategy was applicable (Fig. S1c).

Nitrogen adsorption-desorption tests were carried out for confirmation of the structural changes after the immobilization of ZrGly. A significant increase in surface area of Fe_3O_4 (Fig. 1a) from 14 to 142 $m^2{\cdot}g^{-1}$ was observed in Fe_3O_4@ZrGly (Fig. 1b), indicating the contribution of ZrGly on Fe_3O_4. Besides, Fe_3O_4@ZrGly possessed narrow pore size distribution (Fig. 1b the inset) with smaller mesopores (4.8 nm) compared with Fe_3O_4 (10 nm), which reflected that the introdution of ZrGly nanowires improved the uniformity of the hole of Fe_3O_4. The hierarchical structured organic-metal nanowires with plenty of mesopores can reduce transport limitation [21].

The magnetic properties of Fe_3O_4 and Fe_3O_4@ZrGly were characterized by vibrating sample magnetometry (VSM). The saturation magnetization values of Fe_3O_4 and Fe_3O_4@ZrGly are 31.6 and 25.5 emu·g^{-1}, respectively (Fig. 1c). Though a mild decline of magnetic response was observed after modification, Fe_3O_4@ZrGly maintained enough magnetic

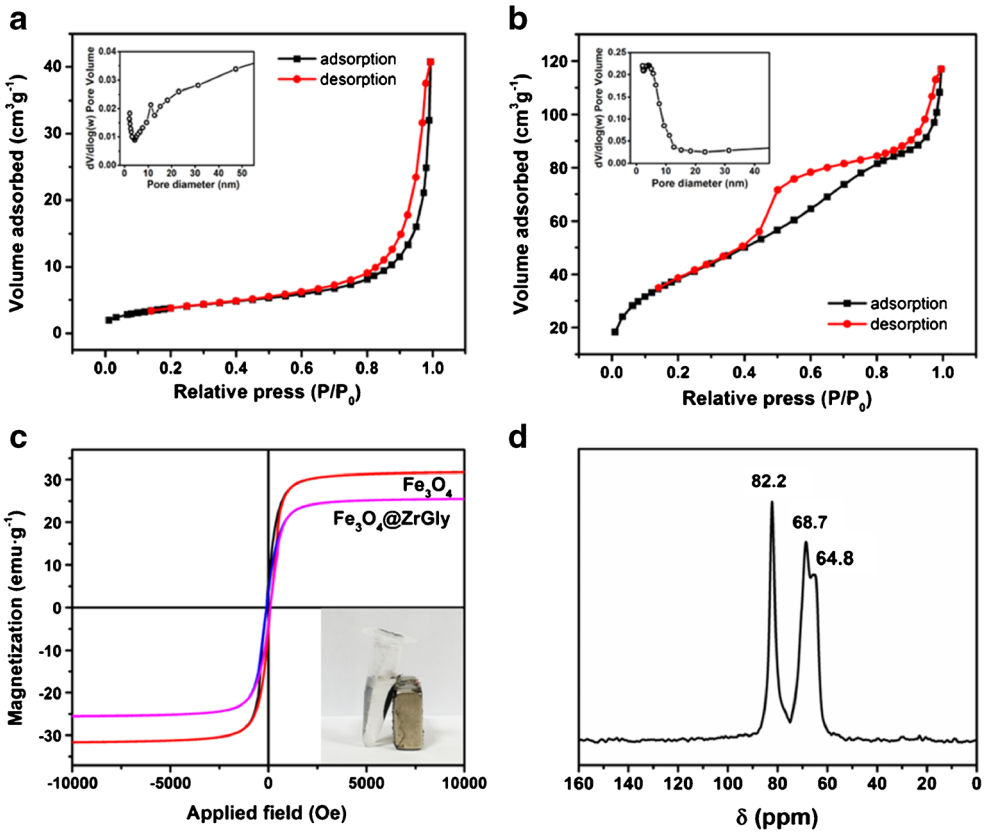

Fig. 1 Nitrogen adsorption-desorption isotherms and pore size distributions (the insets) of (**a**) Fe_3O_4 and (**b**) Fe_3O_4@ZrGly; (**c**) VSM magnetization curves of Fe_3O_4 and Fe_3O_4@ZrGly; (d)Solid state ^{13}C–NMR spectra that were taken from ZrGly nanowires

responsiveness. Hence, it can be isolated from liquid within 30 s by applying an external magnet (Fig. 1c the inset).

Fe_3O_4@ZrGly was also subjected to ATR-FTIR analysis (Fig. S2), and the O-H stretching band in the range of 3000–3500 cm^{-1} and C-H stretching band at 2927–2864 cm^{-1} were also observed in pure ZrGly and Fe_3O_4@ZrGly [22]. The shifting of glycerol peaks in Fe_3O_4@ZrGly from 672 cm^{-1} to 650 cm^{-1} and the reduction of O-H stretching of glycerol in the range of 3500–3000 cm^{-1} indicated the influence of zirconium on O-H of glycerol molecule [23]. Hence, the existence of ZrGly complex on Fe_3O_4 substrate was verified. The composition of Fe_3O_4@ZrGly was also confirmed by TGA analysis (Fig. S3), and the content of glycerol moiety in Fe_3O_4@ZrGly was about 35%.

According to previous research [24], we can predict similar formation mechanism for Fe_3O_4@ZrGly (Scheme 1): during the initial stage of process, zirconium oxyhydrate particles might be generated through alcoholysis reactions or hydrolysis-condensation reactions of zirconium acetylacetonate. This zirconium oxyhydrate on the outer surface of the solid spheres gradually reacted with glycerol to form ZrGly complexes by replacing hydroxyl groups in zirconium oxyhydrate. The formed ZrGly complexes spontaneously nucleated onto the small protuberances which provide many high-energy sites for nanocrystalline growth. As a result, organic-metal nanowires were formed on the surface of Fe_3O_4 because the reaction between polyalcohol with metal ions usually resulted in the formation of 1D coordination complexes [25]. During the pyrolysis step, the outer ZrGly was decomposed to expose the inner zirconium oxyhydrate, which was pyrolyzed afterwards. Accordingly, the Fe_3O_4@ZrGly might have a chain-like coordination structure (Scheme 1) [26]. Most hydroxyl groups of glycerol participated in coordination with zirconium cation, since we selected 2′-deoxycytidine as hydrophilic probe but found no specific adsorption with Fe_3O_4@ZrGly. As shown in Fig. S4, 93% 2′-deoxycytidine still exists in the supernatant solution. The acidic loading environment cripples the coordination interaction between material and 2′-deoxycytidine, and hydroxyl groups of glycerol was suggested participated in the coordination with zirconium cation in Fe_3O_4@ZrGly.

The structures of the prepared organic-metal nanowires and pure ZrGly were examined by ^{13}C solid-state NMR spectroscopy. As shown in Fig. 1d, three relatively broad peaks of carbon atoms in the backbone (δ 68.7 and 64.8 ppm) and side chain (δ 82.2 ppm) are observed and their difference is significant. In fact, the carbon atoms in free glycerol and those bonded directly to oxygen in many other polymeric species, their chemical shifts are all located in the range of 62–74 ppm [27, 28]. The difference of a higher chemical shift for the carbon atoms in the side chain

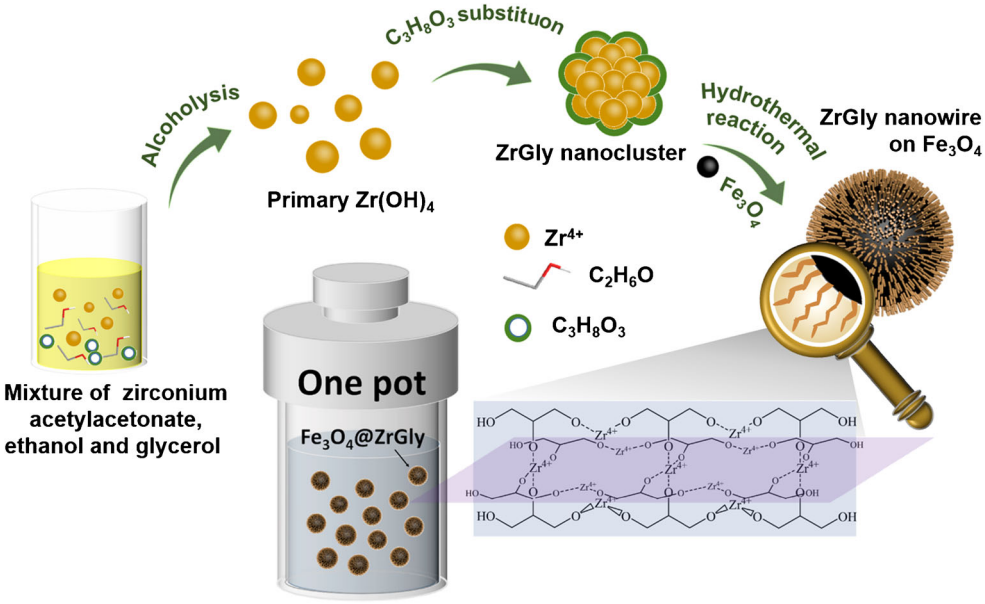

Scheme 1 Schematic illustrations of linear complexes that are formed between glycerol and zirconium cations

of ZrGly owes to the deshielding effect caused by the interaction between zirconium cation and hydroxyl groups. Peaks at 64.8 ~ 68.7 ppm represent the carbon atoms in the backbone. The relatively broad peak we observed here is due to the overlapping between the two peaks of carbon atoms in different chemical environments. The sum intensity of peaks indicated the number of backbone carbons is twice that of the carbon atoms in the side chain, which tallies with the ^{13}C NMR spectra of glycerol. On the other hand, when ZrGly was treated with TFA aqueous solution to wash off the zirconium cation, ^{13}C–NMR analysis of the residue only showed two peaks at 73.0 and 63.5 ppm (Fig. S5). Based on the similarities between our results and standard ^{13}C–NMR spectra of glycerol in the literature, it is evidenced that ZrGly constitutes glycerol which is coordinated with zirconium cation.

Adsorption capacity evaluation and optimization of the immobilization strategy

The data of adsorption experiments were analyzed by the Langmuir and Freundlich adsorption isotherm models (Fig. S6), respectively. Parameters from the fitting of Langmuir and Freundlich adsorption isotherm models are presented in Table 1.

When fitted with Freundlich isotherm eq. (2), the square of determination coefficient (R^2) ranged from 0.88–0.94 for all Fe_3O_4@ZrGlys, 0.99 for commercial ZrO_2, and 0.98 for commercial CeO_2.

$$\log q_e = \frac{1}{n}\log C_e + \log K_F \quad (2)$$

On the other hand, the adsorption isotherm of adenosine on Fe_3O_4@ZrGlys fits well with the Langmuir isotherm (3) ($R^2 > 0.99$), while the linearity of fitting line for the adsorption isotherm on commercial ZrO_2 ($R^2 = 0.94$) or CeO_2 ($R^2 = 0.97$) was lower.

$$\frac{1}{q_e} = \left(\frac{1}{q_{\max} K_L} \times \frac{1}{C_e}\right) + \left(\frac{1}{q_{\max}}\right) \quad (3)$$

These results suggest that Langmuir isotherm model can better reflect the adsorption process of Fe_3O_4@ZrGly. It also points to a monolayer adsorption process. On the other hand, commercial ZrO_2 and CeO_2 behaved just opposite, for which Freundlich isotherm model matches better than Langmuir isotherm model. Based on the ATR-FTIR and TGA results above, active sites of zirconium in Fe_3O_4@ZrGly are occupied by glycerol to a large extent, which causes the active sites on the adsorbent surface becomes identical, resulting in less multilayer adsorption than ZrO_2 and CeO_2. Thus, the Fe_3O_4@ZrGly can capture ribonucleosides through the coordination interaction. It takes place between the residual active sites on ZrGly with the *cis*-diol moieties from ribonucleosides. Interestingly, by raising the molar ratio of zirconium acetylacetonate and glycerol, adsorption capacity of Fe_3O_4@ZrGlys increases at first and then decreases, which is consistent with the change of zirconium content of Fe_3O_4@ZrGlys characterized by EDS (Table. S1 and Fig. S7). Such a decrease in adsorption capacity at low zirconium content may be attributed to the slower growth of nanowires in diluted precursors solution, which resulted in less nanowires deposited on Fe_3O_4. However, in a solution with high concentration of precursors, increased length of nanowires hindered their immobilization on Fe_3O_4. Thus, in order to prepare Fe_3O_4@ZrGly

Table 1 Parameters from the fitting of Langmuir and Freundlich adsorption isotherm models for adenosine on Fe_3O_4@ZrGly, ZrO_2 and CeO_2

Adsorbent	Freundlich model			Langmuir model		
	K_F (mL·μg^{-1})	n	R^2	q_m (mg·g^{-1})	K_L (mL·μg^{-1})	R^2
Fe_3O_4@ZrGly (1:53)[a]	0.67	1.77	0.9312	11.9	0.02	0.9956
Fe_3O_4@ZrGly (1:106)	0.32	2.04	0.9446	36.4	0.04	0.9966
Fe_3O_4@ZrGly (1:264)	4.67	2.56	0.8996	24.2	0.12	0.9995
Fe_3O_4@ZrGly (1:423)	2.94	2.43	0.8815	22.8	0.05	0.9952
ZrO_2	1.28	1.82	0.9943	24.6	0.03	0.9452
CeO_2	0.52	1.68	0.9813	11.6	0.02	0.9768

[a] Ratio in the bracket refers to the molar ratios of zirconium acetylacetonate and glycerol in the reactant

with the highest content of zirconium, the molar ratio of zirconium acetylacetonate and glycerol was optimized as 1:106. The adsorption capacity of Fe_3O_4@ZrGly of optimal composition is calculated as 36 mg·g^{-1}, which is equal to that of commercial ZrO_2. Scatchard plots were also used to calculate binding constant of the adenosine with the Fe_3O_4@ZrGly (1:106), which turned out to be 41 mg/mL (in ESM). However, only 2.2% zirconium was incorporated in the adsorbent, showing the atom economy of the proposal method.

Evaluation of coordination property of Fe_3O_4@ZrGly toward ribonucleosides

Selectivity evaluation

The recognition of *cis*-diols containing ribonucleosides against deoxyribonucleosides was examined to evaluate the enrichment specificity of Fe_3O_4@ZrGly towards cis-diols compounds. As shown in Fig. 2a, in the presence of 500-fold higher amount of deoxyribonucleosides than ribonucleosides, only 1% deoxyribonucleosides are captured by Fe_3O_4@ZrGly. On the other hand, bare Fe_3O_4 showed poor affinity towards ribonucleosides or deoxyribonucleosides, indicating that immobilizing ZrGly on Fe_3O_4 played a key role in the coordination enrichment of ribonucleosides. Furthermore, glucose and HRP were chosen as the representative of different saccharide and glycoproteins to intervene the enrichment of ribonucleosides. Changes of the recovery of adenosine were compared, since glucose and HRP didn't absorb the ultraviolet light. The results indicated that the recovery of ribonucleotides only reduced around 10% in presence of 100-fold higher amount of glucose and HRP (Fig. 2b, c), which suggested that Fe_3O_4@ZrGly had high selectivity for ribonucleosides mediately.

Methodological evaluation

After extraction optimization, 0.5% $NH_3·H_2O$ (v%) was used as sampling solution and 0.1% FA (v%) was used as desorption solution to achieve the best performance. Under the optimal conditions, Fe_3O_4@ZrGly was applied to selective capture of four ribonucleosides (cytidine, uridine, guanosine and adenosine) from human urine. As shown in Table. S2, the limits of detection (LODs) and limits of quantification (LOQs) were in the range of 1.7–19 ng·mL^{-1} and 5.1–58 ng·mL^{-1}, respectively. As shown in Table. S3, the intra- and inter-day relative standard deviations (RSDs) were below 12.4% and 11.2%, illustrating that the reproducibility of the present method was acceptable. The recoveries were measured by analyzing the spiked human urine at three different concentrations ranging from 0.2 to 10.0 μg·mL^{-1}. The results showed that the recoveries were in the range of 90.6–115%. The variation of batch-to-batch was investigated by comparing the recovery of four ribonucleosides with three batches of

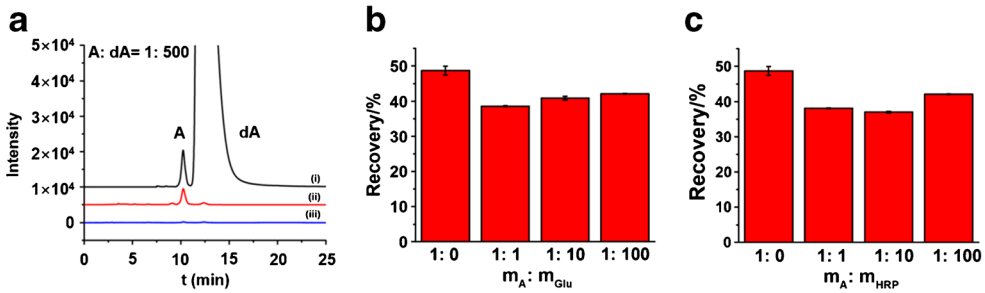

Fig. 2 **a** LC-UV chromatograms of adenosine (A) and 2′-deoxyadenosine (dA) enrichened with different materials ((i) before enrichment, (ii) after enrichment with Fe_3O_4@ZrGly, (iii) after enrichment with Fe_3O_4); Recovery of adenosine in the presence of different amount of (**b**) glucose and (**c**) HRP. The amount of adenosine was 0.2 μg, the detection wavelength was set at 254 nm

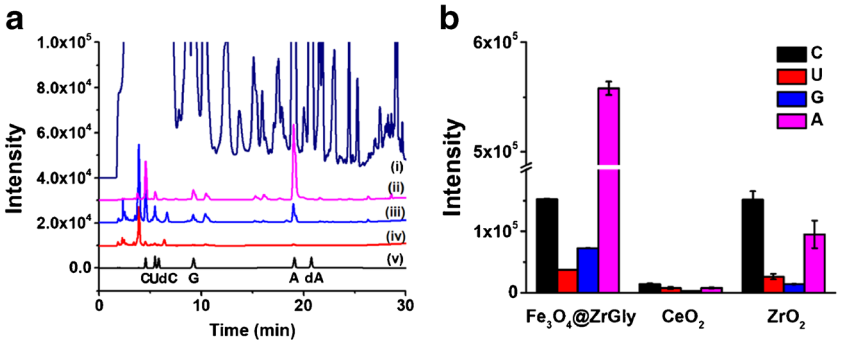

Fig. 3 **a** LC-UV chromatograms of adenosine, cytidine, guanosine, uridine, 2′-deoxyadenosine, 2′-deoxycytidine in urine sample. (i) direct analysis of a spiked urine sample; (ii) spiked urine sample after enrichment with Fe_3O_4@ZrGly; (iii) spiked urine sample after enrichment with ZrO_2; (iv) spiked urine sample after enrichment with CeO_2; (v)direct analysis of ribonucleoside standards (5 μg·mL^{-1}, the detection wavelength was set at 254 nm)

Fe_3O_4@ZrGly. The result showed that the relative standard deviations were 3.1–9.6%, indicating that the Fe_3O_4@ZrGly possess good reproducibility.

A comparison between this method and reported methods is presented in Table S4. It was observed that this method had comparable LODs and consumed less adsorbent. In addition, we made the comparison among of Fe_3O_4@ZrGly, ZrO_2 and CeO_2 for the enrichment of spiked ribonucleosides in urine samples. The intensity of four ribonucleosides were much higher in spiked urine extraction by Fe_3O_4@ZrGly without serious interference and nonspecific adsorption (Fig. 3a, b). Because the zirconium ions in Fe_3O_4@ZrGly mostly participate in the coordination with glycerol, the residual coordination sites are identical, which endows Fe_3O_4@ZrGly high selectivity and less nonspecific adsorption. On the other hand, ZrO_2 has 8 different coordination sites and impurities in urine matrix may shield these sites and attenuate its enrichment performance. Besides, the adsorption capacity of the CeO_2 is too low to deal with the complicated interference in urine matrix (Table 1). Conclusively, Fe_3O_4@ZrGly has shown the best purification capability of ribonucleosides from complex samples.

Real sample analysis

To demonstrate the applicability of the developed method, Fe_3O_4@ZrGly was applied on the analysis of two urine samples that were collected from two healthy people. The average levels of adenosine, cytidine, guanosine and uridine excreted were normalized by the concentrations of creatinine in urine samples. As shown in Table 2, the prepared material has facilitated effective enrichment of ribonucleosides. The developed method enabled sensitive and accurate measurements of ribonucleosides in urine of different people. Consequently, our method can satisfy the need of clinical detection.

Conclusion

In summary, we have developed a novel strategy for the synthesis of hierarchical Fe_3O_4@ZrGly. The dissolution-recrystallization formation mechanism and the structure of Fe_3O_4@ZrGly were well verified. In contrast to the multilayer adsorption mechanism of commercial ZrO_2, Fe_3O_4@ZrGly tended to adsorb adenosine in monolayer and the adsorption capacity was calculated as 36 mg·g^{-1}. Finally, Fe_3O_4@ZrGly was also utilized in the selective enrichment of ribonucleosides from urine samples. This versatile approach presented a new and promising protocol for the immobilization of organic-metal nanowires on materials for the applications in metabolomics research. However, Fe_3O_4@ZrGly had no advantage on adsorption capacity compared with our previous work [29], since active sites of zirconium in Fe_3O_4@ZrGlys are occupied by glycerol to a large extent. Thus the Fe_3O_4@ZrGly is limited on application for modified ribonucleosides with extremely low concentration in complicated biological samples. We will further try to settle this issue and improve the method.

Table 2 Average ribonucleoside levels excreted in urine samples from a normal subject

	A(nmol·mmol creatinine^{-1})	C(nmol·mmol creatinine^{-1})	G(nmol·mmol creatinine^{-1})	U(nmol·mmol creatinine^{-1})
Sample 1	344 ± 5.1	70.9 ± 6.7	42.9 ± 1.7	98.6 ± 5.8
Sample 2	256 ± 1.9	117 ± 8.5	55.3 ± 3.7	36.5 ± 6.1

Acknowledgements The authors thank the financial support from the National Basic Research Program of China (973 Program) (2013CB910702), the National Natural Science Foundation of China (21475098, 2163506, 31670373).

Compliance with ethical standards The author(s) declare that they have no competing interests.

References

1. Shao Y, Zhu B, Zheng R, Zhao X, Yin P, Lu X, Jiao B, Xu G, Yao Z (2015) Development of urinary pseudotargeted LC-MS-based metabolomics method and its application in hepatocellular carcinoma biomarker discovery. J Proteome Res 14(2):906–916
2. Kobayashi Y (2014) High-performance lectin affinity chromatography. Methods Mol Biol 1200:69–77
3. Boulton M, Jones A, Walker R (1971) Synthetic analogues of polynucleotides. VI. The synthesis of ribonucleoside dialdehyde derivatives of polyacrylic acid hydrazide and their interaction with polynucleotides. Biochim Biophys Acta 246(2):197–205. https://doi.org/10.1016/0005-2787(71)90128-6
4. Dai Q, Ma J, Ma S, Wang S, Li L, Zhu X, Qiao X (2016) Cationic ionic liquids organic ligands based metal-organic frameworks for fabrication of core-shell microspheres for hydrophilic interaction liquid chromatography. ACS Appl Mater Interfaces 8(33):21632–21639
5. Liu Y, Ren L, Liu Z (2011) A unique boronic acid functionalized monolithic capillary for specific capture, separation and immobilization of cis-diol biomolecules. Chem Commun (Camb) 47(17):5067–5069
6. Cheng T, Zhang Y, Liu X, Zhang X, Zhang H (2017) A filter paper coated with phenylboronic acid-modified mesoporous silica for enrichment of intracellular nucleosides prior to their quantitation by HPLC. Microchim Acta 184(10):4007–4013
7. Cheng T, Zhang Y, Liu X, Zhang X, Zhang H (2017) Surfactant assisted enrichment of nucleosides by using a sorbent consisting of magnetic polysulfone capsules and mesoporous silica nanoparticles modified with phenylboronic acid. Microchim Acta 184(1):271–278
8. Jiang G, Zhu W, Shen X, Xu L, Li X, Wang R, Liu C, Zhou X (2017) Colorimetric and visual determination of adenosine triphosphate using a boronic acid as the recognition element, and based on the deaggregation of gold nanoparticles. Microchim Acta 184(11):4305–4312
9. Li H, Zhu S, Cheng T, Wang S, Zhu B, Liu X, Zhang H (2016) Binary boronic acid-functionalized attapulgite with high adsorption capacity for selective capture of nucleosides at acidic pH values. Microchim Acta 183(5):1779–1786
10. Sun X, Ma R, Chen J, Shi Y (2017) Boronate-affinity based magnetic molecularly imprinted nanoparticles for the efficient extraction of the model glycoprotein horseradish peroxidase. Microchim Acta 184(10):3729–3737
11. Wang H, Feng W, Jia Q (2015) A graphene oxide functionalized with 3-aminophenylboronic acid for the selective enrichment of nucleosides, and their separation by capillary electrophoresis. Microchim Acta 182(1):185–192
12. Chu J, Qi C, Huang Y, Jiang H, Hao Y, Yuan B, Feng Y (2015) Metal oxide-based selective enrichment combined with stable isotope labeling-mass spectrometry analysis for profiling of ribose conjugates. Anal Chem 87(14):7364–7372
13. Ahmadi M, Elmongy H, Madrakian T, Abdel-Rehim M (2017) Nanomaterials as sorbents for sample preparation in bioanalysis: a review. Anal Chim Acta 958:1–21
14. Jamshaid T, Neto E, Eissa M, Zine N, Kunita M, El-Salhi A, Elaissari A (2016) Magnetic particles: from preparation to lab-on-a-chip, biosensors, microsystems and microfluidics applications. Trac-Trend Anal Chem 79:344–362
15. Park S, Choi K, Lee S, Oh I, Park S, Park H (2017) CNT branching of three-dimensional steam-activated graphene hybrid frameworks for excellent rate and cyclic capabilities to store lithium ions. Carbon 116:500–509
16. Qian X, Xu Q, Hang T, Shanmugam S, Li M (2017) Electrochemical deposition of Fe3O4 nanoparticles and flower-like hierarchical porous nanoflakes on 3D cu-cone arrays for rechargeable lithium battery anodes. Mater Design 121:321–334
17. Bian X, Hong K, Ge X, Song R, Liu L, Xu M (2015) Functional hierarchical nanocomposites based on ZnO nanowire and magnetic nanoparticle as highly active recyclable photocatalysts. J Phys Chem C 119(4):1700–1705
18. Yuan J, Schmalz H, Xu Y, Miyajima N, Drechsler M, Moeller M, Schacher F, Mueller A (2008) Room-temperature growth of uniform tellurium nanorods and the assembly of tellurium or Fe3O4 nanoparticles on the nanorods. Adv Mater 20(5):947–94+
19. Ding J, Gao Q, Luo D, Shi Z, Feng Y (2010) N-Octadecylphosphonic acid grafted mesoporous magnetic nanoparticle: preparation, characterization, and application in magnetic solid-phase extraction. J Chromatogr A 1217(47):7351–7358
20. Ren L, Liu Z, Dong M, Ye M, Zou H (2009) Synthesis and characterization of a new boronate affinity monolithic capillary for specific capture of cis-diol-containing compounds. J C hromatogr A 1216(23):4768
21. Tian G, Chen Y, Zhou W, Pan K, Tian C, Huang X, Fu H (2011) 3D hierarchical flower-like TiO_2 nanostructure: morphology control and its photocatalytic property. CrystEngComm 13(8):2994–3000
22. Indran V, Syuhadazuhaimi N, Deraman M, Maniam G, Yusoff M, Yunhin TY, Ab. Rahim M (2014) An accelerated route of glycerol carbonate formation from glycerol using waste boiler ash as catalyst. RSC Adv 4 (48):25257
23. Remias R, Kukovecz A, Daranyi M, Kozma G, Varga S, Konya Z, Kiricsi I (2009) Synthesis of zinc glycerolate microstacks from a ZnO nanorod sacrificial template. Eur J Inorg Chem 24:3622–3627
24. Zhang J, Wang Y, He Y, Jiang T, Yang H, Tan X, Kang R, Yuan Y, Shi L (2010) Determination of urinary adenosine using resonance light scattering of gold nanoparticles modified structure-switching aptamer. Anal Biochem 397(2):212–217
25. Wang Y, Jiang X, Xia Y (2003) A solution-phase, precursor route to polycrystalline SnO_2 nanowires that can be used for gas sensing under ambient conditions. J Am Chem Soc 125(52):16176–16177
26. Jiang X, Wang Y, Herricks T, Xia Y (2004) Ethylene glycol-mediated synthesis of metal oxide nanowires. J Mater Chem 14(4):695–703
27. Lopes T, Ribeiro M, Ming C, Grimaldi R, Goncalves L, Marsaioli A (2016) Comparison of the regiospecific distribution from triacylglycerols after chemical and enzymatic interesterification of high oleic sunflower oil and fully hydrogenated high oleic sunflower oil blend by carbon-13 nuclear magnetic resonance. Food Chem 212:641–647
28. Merchak N, Silvestre V, Loquet D, Rizk T, Akoka S, Bejjani J (2017) A strategy for simultaneous determination of fatty acid composition, fatty acid position, and position-specific isotope contents in triacylglycerol matrices by C-13-NMR. Anal Bioanal Chem 409(1):307–315
29. He H, Sun Y, Li B, Yu Q, Wang T, Feng Y (2013) Boronate affinity solid-phase extraction based on functionalized magnesia-zirconia composite for enrichment of nucleosides in human urine. Anal Methods 5(6):1435–1441